Available online at www.sciencedirect.com
SCIENCE DIRECT®
Thermochimica Acta 414 (2004) 79–84
thermochimica acta
www.elsevier.com/locate/tca

Oxidation behaviour and kinetic properties of shape memory $CuAl_xNi_4$ ($x = 13.0$ and 13.5) alloys

R. Zengin*, S. Ozgen, M. Ceylan

Department of Physics, Faculty of Arts and Sciences, Firat University, 23169 Elazig, Turkey

Received 2 July 2003; received in revised form 18 November 2003; accepted 24 November 2003

Abstract

Although the copper-based shape memory alloys (SMA) have some important problems such as controlling of the kinetic properties in the shape memory ability, they have relatively more advantages when compared to nitinol, such as lower price and simpler production technology. In order to determine the kinetic properties and oxidation rates of shape memory $CuAl_xNi_4$ ($x = 13$ and 13.5) alloys with polycrystalline forms, the alloys have been homogenized in β-phase field at 930 °C for 30 min and immediately quenched in iced-brine water at −3 °C. The transformation temperatures in a period of three thermal cycles which include heating and cooling processes have been determined through Shimadzu DSC-50 differential scanning calorimeter. Activation energies of forward and reverse martensitic transformations have been calculated by using the Kissenger method. Thermogravimetric analysis with Shimadzu TGA-50 have been carried out for the determination of mass changes of alloys during heating and cooling cycles with two temperature rates selected as 10 and 30 °C/min up to 900 °C. It has been shown that increasing aluminium content reduces the oxidation rates of the alloys. It has also been established that CuAlNi shape memory alloys have a good stabilization in martensitic phase.

Keywords: Shape memory effect; Transformation temperatures; Activation energy; Oxidation behaviour

1. Introduction

Shape memory effect is related to the thermoelastic martensitic transformations. It is implicit in the concept of thermoelastic transformation that there is reversible behaviour involved in the martensite ↔ austenite transformations [1,2]. Therefore, reversible transformation occurs on heating an alloy, martensitic transformation advances with the formation of the martensite plates and the earlier formed plates vanish later during the reverse transition on heating. After an alloy which exhibits thermoelastic martensitic transition is deformed at a temperature below M_f where the martensitic transition completes, even if the deformation stresses are removed, it remains at the deformed shape but recovers the original shape on heating over the austenite phase finish temperature (A_f) and gains the deformed shape on re-cooling below M_f. These shape changes reoccur during the cycles of heating and cooling in martensitic region and a usable force arises. This behaviour and these alloys are called as two way shape memory effect (TWME) and shape memory alloys (SMAs), respectively [2–4]. These alloys can be used as components in some devices used in wide variety of applications such as biomechanics, vibration control, medicine, industry and aerospace engineering [5–7]. Binary NiTi and ternary Cu-based SMAs are widely used in these applications. Although the Cu-based SMAs have the advantage of a lower price, there are very important problems such as martensite stabilization [1,8] and transformation temperatures [9–11], particularly in CuZnAl SMAs. The ternary CuAlNi SMAs alternative to CuZnAl alloys exhibit the TWME in a wide composition range of alloying elements, nickel or aluminium [12]. However, compositional variations in these alloys can modify not only the transformation temperatures; but also lead to the deterioration of the ductility. They may even result in the loss of thermoelastic and other properties during thermal cycling [13]. Therefore, for efficient use of these alloys in the technological applications, the knowledge of the changes in transformation temperatures with both composition and thermal cycling is very important. Besides, in the case of the use of SMAs at high temperatures, the changes of oxidation rates with heating and cooling rates must also be known.

* Corresponding author. Tel.: +90-4242370000; fax: +90-4242330062.
E-mail address: rzengin@firat.edu.tr (R. Zengin).

0040-6031/$ – see front matter © 2003 Elsevier B.V. All rights reserved.
doi:10.1016/j.tca.2003.11.020

The studies on the problems of Cu-based ternary SMAs have been generally on single crystals of the alloys [8,10,11] but the studies on polycrystalline alloys are limited in literature. Therefore, we have planned to investigate the CuAlNi alloys in polycrystalline forms which have two different compositions with constant nickel and 13.0 and 13.5 at.% of aluminium. In addition to the thermogravimetric analysis with two different heating and cooling rates, the differential scanning calorimetric (DSC) investigations have been performed on the alloys in the period of three thermal cycles. The kinetic parameters related to the shape memory ability of the alloys have been calculated by the method of Kissinger [14,15].

2. Experimental

Two CuAlNi alloys which exhibit TWME have been supplied by The Scientific and Technical Research Council of Turkey (TUBITAK). These alloys have been received in the cylindrical ingot in 1 cm diameter and 10 cm long. The chemical compositions and electron/atom (*e*/*a*) ratios of the alloys labelled as A1 and A2 specimens are given in Table 1.

The specimens were cut in the disc form with 2 mm in thickness and then divided into nine pieces by cutting with a saw. The specimens were obtained from a region at the near centre of these discs in approximately dimensions of 2 mm × 3 mm × 2 mm. These specimens were put into quartz tubes, treated by solution and evacuated to homogenize in austenitic conditions at 930 °C for 30 min. Homogenised specimens, then, were immediately quenched in iced-brine water at −3 °C to obtain β-type martensite. After these treatments, the calorimetric experiments were performed by means of Shimadzu DSC-50 instrument at a rate of 10 °C/min between room temperature and 200 °C. Each heating and cooling cycle was also individually repeated three times by the DSC instrument for A1 (132 mg) and A2 (105 mg) specimens. The cooling treatments were acted by using liquid nitrogen.

In order to determine the mass changes upon heating and cooling the specimens between room and betatizing temperatures at free atmosphere, the specimens of 27.9 mg for A1 and 56.7 mg for A2 were firstly heated from room temperature to 900 °C at two different heating rates of 10 and 30 °C/min and then left to cool to room temperature by themselves. The thermogravimetric experiments for this purpose were performed by means of Shimadzu TGA-50 instrument.

Table 1
Alloys compositions in wt.%, at.% and *e*/*a* ratios

Alloy	wt.%			at.%			*e*/*a*
	Cu	Al	Ni	Cu	Al	Ni	
A1	83.0	13.0	4.0	70.38	25.95	3.67	1.55
A2	82.5	13.5	4.0	69.56	26.80	3.64	1.57

3. Results and discussion

3.1. DSC analysis

The DSC curves obtained from the three thermal cycling on A1 and A2 specimens are shown in Fig. 1(a) and (b). The start (subscribed by s), finish and maximum (subscribed by p) temperatures of forward and reverse transformations and other calculated properties, such as heat and activation energy of transformations and hysteresis ($\Delta T = A_p - M_p$), from these DSC curves are given in Table 2. The activation energies have been calculated from the obtained characteristic temperatures of the forward and reverse transformations using the Kissinger method described as

$$\ln\left[\frac{\phi}{T_m^2}\right] = C - \frac{E_a}{RT_m} \quad (1)$$

Here ϕ is the heating rate, T_m the maximum peak temperature (A_p or M_p), C the integration constants, E_a the activation energy, and R the universal gas constant [14]. The activation energies in the first cycles for A1 and A2 are calculated as 23.03 ± 0.02 and 16.94 ± 0.03 kJ/mol, respectively. From these values, it can be said that an increase order of 3.7% in aluminium content of the alloy with constant nickel causes the decrease in activation energy by 26.5 ± 0.2%.

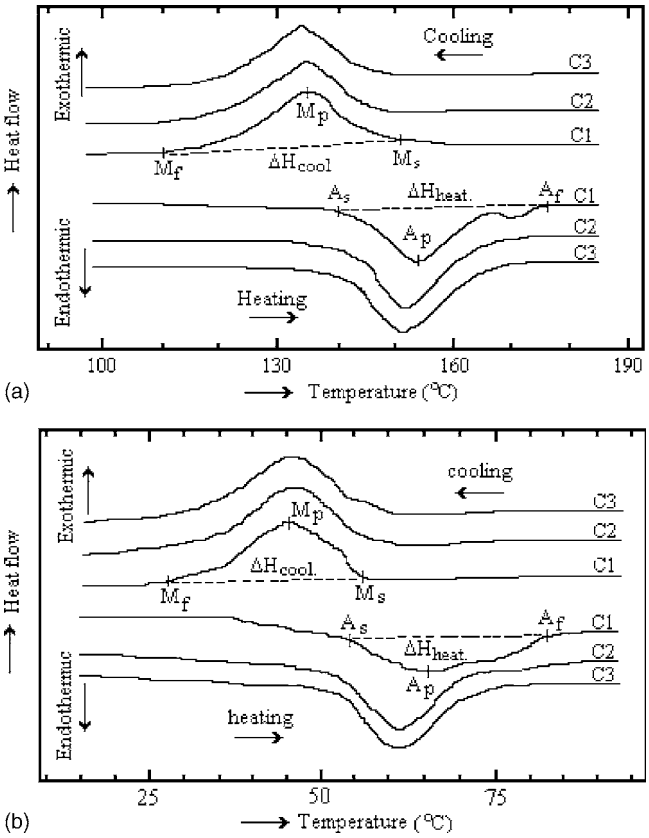

Fig. 1. The DSC curves plotted for (a) A1 and (b) A2 specimens. C1–C3 denoted first, second and third cycles, respectively.

Table 2
The characteristic temperatures obtained by DSC investigations for A1 and A2 specimens and the calculated quantities for thermoelastic transformations

Alloy	Cycle	A_s (°C)	A_p (°C)	A_f (°C)	M_s (°C)	M_p (°C)	M_f (°C)	ΔH_{heat} (J/g)	ΔH_{cool} (J/g)	ΔT (°C)	$E_a^{A\rightarrow M}$ (kJ/mol)	$E_a^{M\rightarrow A}$ (kJ/mol)
A1	1	139.9 ± 0.4	155.1 ± 0.3	176.3 ± 0.4	150.6 ± 0.4	135.8 ± 0.3	110.1 ± 0.4	−5.91 ± 0.13	6.20 ± 0.12	19.3 ± 0.6	23.03 ± 0.02	21.68 ± 0.02
	2	135.8 ± 0.2	153.1 ± 0.2	172.3 ± 0.2	150.6 ± 0.4	135.8 ± 0.2	110.1 ± 0.4	−6.49 ± 0.07	6.51 ± 0.12	17.3 ± 0.4	22.89 ± 0.01	21.68 ± 0.01
	3	135.4 ± 0.2	152.3 ± 0.2	172.5 ± 0.2	150.9 ± 0.4	133.5 ± 0.2	112.7 ± 0.4	−6.45 ± 0.07	6.42 ± 0.13	18.8 ± 0.4	22.84 ± 0.02	21.52 ± 0.02
A2	1	52.1 ± 0.4	66.2 ± 0.4	83.4 ± 0.4	55.4 ± 0.4	44.7 ± 0.3	25.9 ± 0.4	−5.09 ± 0.13	6.04 ± 0.16	21.5 ± 0.7	16.94 ± 0.03	15.52 ± 0.02
	2	50.3 ± 0.2	60.3 ± 0.2	73.0 ± 0.2	57.7 ± 0.4	45.0 ± 0.4	28.7 ± 0.4	−4.34 ± 0.07	5.85 ± 0.16	15.3 ± 0.6	16.55 ± 0.01	15.54 ± 0.02
	3	49.7 ± 0.2	59.9 ± 0.2	72.8 ± 0.2	59.2 ± 0.4	45.3 ± 0.4	26.7 ± 0.4	−4.38 ± 0.07	6.03 ± 0.15	14.6 ± 0.6	15.86 ± 0.02	15.56 ± 0.02

It has been seen from Fig. 1(a) and (b) that the characteristic transformation temperatures and hysteresis decrease with the increasing number of thermal cycling. The decreases of the characteristic temperatures are attributed to the microstructural changes of martensite [1,16]. In particularly, the observed decreases in the A_s and A_f reverse transformation temperatures can be attributed to the dislocations formed by the cycling effect. This means that the alloys have the most stable state at the initial stage and lose the stability with further cycles [1,17]. The cycles of the shape memory alloys can be regarded as non-isothermal ageing at a certain temperature interval. The changes in the transition temperatures for the first, second and third cycles are shown in Fig. 1(a) and (b) and their peak values are given in Table 2. DSC curves belonging to the first cycle have a broad temperature range which is centred at 155.1 ± 0.3 and $66.2 \pm 0.4\,^{\circ}C$ for the A1 and A2 specimens, respectively, while latter cycle peaks are narrower than the formers.

The hysteresis values are calculated as 19.3 ± 0.6 and $21.5 \pm 0.7\,^{\circ}C$ for A1 and A2 alloys, respectively, in the first cycles. Such a small hysteresis is one of the typical characteristics of thermoelastic martensitic transformations. The existing models on these transformations treat the nucleation process as a stage in the transformation that occurs rapidly in a way similar to a shear, whose activation energy is very small [18]. The detailed analysis on the martensitic structures and thermodynamic properties of the specimens can be found elsewhere [19]. We rather focussed on the cause of the oxidation behaviours of the alloys in this study.

3.2. TGA analysis

The mass change curves obtained from thermogravimetry experiments are shown in Fig. 2(a) and (b) for A1 and A2 specimens, respectively. At the lower sides in these figures, the curves obtained with the heating rates of $10\,^{\circ}C$/min and with the cooling are shown and those of $30\,^{\circ}C$/min are in the upper sides.

In these experiments the alloys have been heated from room temperature to $900\,^{\circ}C$ which is near the betatizing temperature ($930\,^{\circ}C$) and, then, cooled to room temperature at free atmosphere. The mass augmentations of the A1 and A2 specimens have been obtained as 0.37 ± 0.01 and $0.22 \pm 0.01\%$, respectively, during the heating regimes of $10\,^{\circ}C$/min and the mass augmentation rates corresponding to this percentages are calculated as $(1.94 \pm 0.20) \times 10^{-3}$ mg/min for A1 and $(2.12 \pm 0.20) \times 10^{-3}$ mg/min for A2. Also, this mass augmentation rates correspond to the oxidation rates of $1.21 \pm 0.04 \times 10^{15}$ oxygen/s for A1 and $(1.33 \pm 0.04) \times 10^{15}$ oxygen/s for A2. The mass increases in the cooling regimes are $0.17 \pm 0.01\%$ for A1 and $0.09 \pm 0.01\%$ for A2. Hence, total mass augmentations for the rate of $10\,^{\circ}C$/min are calculated as 0.54 ± 0.02 and $0.31 \pm 0.02\%$ for A1 and A2 specimens, respectively.

The values obtained from the experiments with the heating rate of $30\,^{\circ}C$/min are $0.09 \pm 0.01\%$ in the heating regime

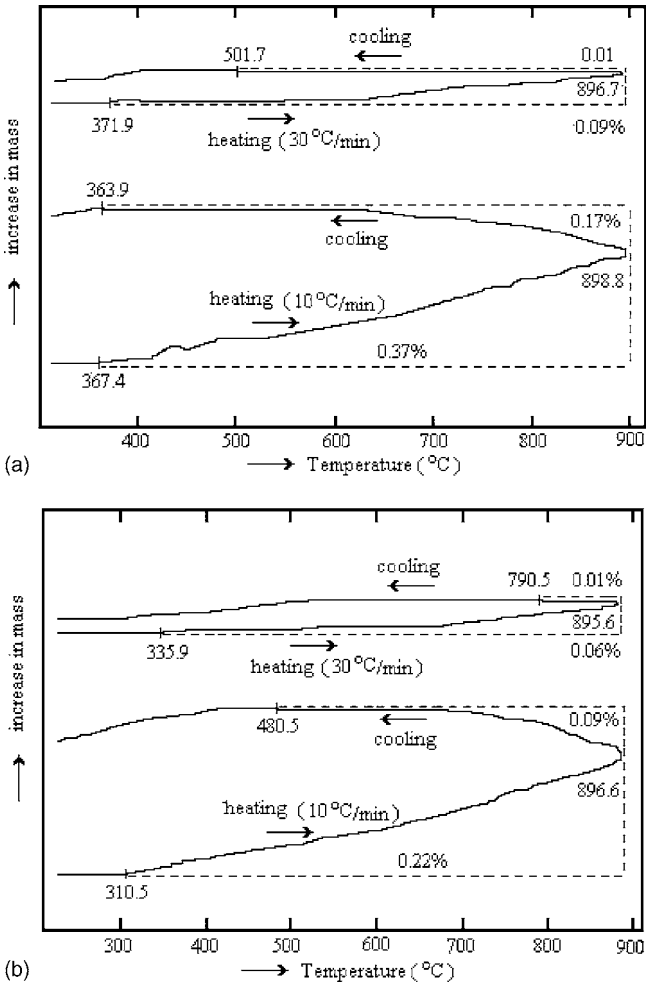

Fig. 2. The TGA curves plotted for (a) A1 and (b) A2 specimens. The curves obtained by the high heating rates are shown at the top of the figures.

and $0.01 \pm 0.01\%$ in the cooling regime for A1 specimen, and 0.06 ± 0.01 and $0.01 \pm 0.01\%$ for A2 specimen. The mass augmentation rates corresponding to these percentages in the heating regimes are $(1.43 \pm 0.20) \times 10^{-3}$ mg/min for A1 and $(1.82 \pm 0.30) \times 10^{-3}$ mg/min for A2. This mass augmentation rates also correspond to $(0.91 \pm 0.04) \times 10^{15}$ oxygen/s for A1 and $(1.14 \pm 0.04) \times 10^{15}$ oxygen/s for A2. Total mass augmentations during heating/cooling regimes with this rate are $0.10 \pm 0.02\%$ for A1 and $0.07 \pm 0.02\%$ for A2. It can be concluded that these increase in mass are caused by oxidation upon heating.

It can be seen from Fig. 2 that heating with the rate of $10\,^{\circ}C$/min up to $367.4 \pm 0.2\,^{\circ}C$ for A1 and $310.5 \pm 0.2\,^{\circ}C$ for A2 has not caused important mass increases. The specimens start to capture the oxygen atoms at these temperatures which are important in the technological applications because the SMAs lose most of own shape memory properties. The temperatures where the oxidation is stopped in cooling processes are also determined as $363.9 \pm 0.2\,^{\circ}C$ for A1 and $480.5 \pm 0.2\,^{\circ}C$ for A2. The starting temperatures for

oxidation during the heating processes with 30 °C/min rate are obtained as 371.9 ± 0.2 °C for A1 and 335.9 ± 0.2 °C for A2 specimens. In the cooling regime, the finishing oxidation temperatures are also obtained as 501.7 ± 0.2 °C for A1 and 790.5 ± 0.2 °C for A2 specimens. At these temperatures, oxygen atoms do not find the activation energy to diffuse into the specimens. It is well known that the SMAs are generally used under thermal treatments and cycling. Therefore, this information on the oxidation behaviour of the alloys used in this study can become useful for heat treatments.

3.2.1. The effects of aluminium content on oxidation behaviour

The polycrystalline alloys always present intergranular failure; in some cases the cause of this failure has been attributed to the presence of the brittle γ_2 phase (Cu_9Al_4) at grain boundaries [20]. The grain boundaries in polycrystalline alloys serve as a region trapping oxygen atoms and enhance the oxidation in metals and alloys [21,22]. Therefore, the oxidation rate strongly depends on the properties of alloy surfaces and so the surfaces of the specimen must be carefully prepared [21]. Besides, the oxidation of two CuNiAg alloy systems in air has been investigated at 600–700 °C by Niu et al. [23] and they have shown that the two alloy systems form complex scales containing an outermost layer of CuO followed by an inner region composed of a mixture of Cu_2O plus NiO with a number of silver metal particles. The alloys used in our study may be compared with those of Niu et al. due to the structural similarities, both the alloy systems have a Cu-rich β phase field, polycrystalline structure, and approximately equal atomic radius and ionic radius which are important for oxidation [21].

In the present study, we have attentively prepared the surfaces of the specimens. The surfaces of the A1 and A2 specimens have the grain boundaries with approximately same order of size [19]. Due to the γ_2 phase at the grain boundaries, we may conclude that the oxidation in the specimens begin at the grain boundaries and progress with occurring CuO, AlO, Cu_2O and a few of NiO reactions. These oxides may be formed as complex scales containing an outermost layer of CuO followed by an inner region composed of a mixture of Cu_2O plus AlO with a number of NiO.

In order to realize the effect of aluminium content on the oxidation behaviour of the alloy, we have calculated the oxygen absorption rate per mass and have found it to be $(4.36 \pm 0.02) \times 10^{13}$ oxygen/mg s for A1 and $(2.34 \pm 0.02) \times 10^{13}$ oxygen/mg s for A2 at 10 °C/min. These values show that the increasing aluminium content causes decrease in the oxidation rate. Therefore, increasing aluminium content can cause decrease in Cu_2O and NiO formations in the inner regions even if it is not possible on the outermost layer. Hence, incoming oxygen atoms into the inner region may be prevented by the aluminium oxide formations on the outer layer because of the lower reaction energy of AlO than the other oxide reactions. Copper atoms cannot be oxidized initially during the earlier stages of treatment, because of the higher Gibbs free energy for the formation of copper oxide relative to that for the formation of alumina [24].

Another observation on the oxidation behaviour of the specimens is that the difference between oxidation start temperatures depends on the aluminium content. The oxidation start temperature of the specimen with high aluminium content is relatively lower than the specimen with low aluminium content. This situation can be explained because the reaction energy of AlO is lower than the other oxide reactions. So, in the A2 specimen with high aluminium content, the oxidations easily start on the outermost layer and the aluminium oxide layer easily grow [21,25]. However, once the aluminium oxide layer occurs it does not allow the oxygen atoms to diffuse into the inner region. So, the aluminium content inhibits the oxidation of the copper.

Therefore, it can be concluded that the increase of the aluminium content in the used alloys reduce the oxidation rate. Also, in a study on the enhancement of oxidation resistance in Cu and Cu(Al) thin layers, Horvath et al. [25] obtained the similar results that the presence of aluminium and the implantation together give increased protection against oxidation of CuAl alloys.

3.2.2. The effects of heating rate on oxidation behaviour

The oxidation rate of the A1 specimen is reduced from $(4.36 \pm 0.02) \times 10^{13}$ oxygen/mg s to $(3.22 \pm 0.02) \times 10^{13}$ oxygen/mg s by changing the heating rate from 10 to 30 °C/min. With the same way, the oxidation rate of the A2 specimen is reduced from $(2.34 \pm 0.02) \times 10^{13}$ oxygen/mg s to $(2.01 \pm 0.02) \times 10^{13}$ oxygen/mg s. These decrease in the oxidation rates must be interpreted by taking into account the time consumed during heating process, that is, the specimens have more time in lower heating rates than the higher heating rates for the oxide formations.

The oxidation mechanism of the pure copper is explained in two stages [25]: firstly, a thin layer of Cu_2O forms on the surface. This oxide film is usually stressed or porous, because the molar volume of the Cu_2O phase is much higher than that of copper. Secondly, the oxygen rich CuO forms under the Cu_2O oxide film but this formation is usually a slower process at lower temperatures. However, in the case of low-aluminium-alloyed copper, it is found that the CuO phase forms first and then the Cu_2O phase [23,25]. This process can be seen from the TGA curves in Fig. 2a obtained for A1 specimen. In the figure, the mass augmentation for 10 °C/min heating rate exhibit a fluctuation at the temperature range of (367.4 ± 0.2)–(500.0 ± 0.2) °C. However, this fluctuation is suppressed by increasing the heating rate to 30 °C/min. Therefore, it can be said that, at lower heating rate, the oxidation is started by forming the CuO and Cu_2O phases together and enhanced by growing the copper oxide but at higher heating rates, the Cu_2O phase is inhibited by not giving more time required for the formation. Another important mechanism inhibiting the formation of Cu_2O phase is the alloyed impurities occupying the vacancy sites at the grain boundaries. Also, the increase of heating

rate causes the activation of the atomic migration, particularly at the grain boundaries. The same interpretations can be made on the results from A2 specimen, except for Cu_2O phase formation during earlier stages of oxidation. In Fig. 2b, it is seen that the obtained curve is nearly linear and the fluctuations do not occur in earlier and latter stages of the oxidation. This observation shows that the Cu_2O phase formation is suppressed by the alloying elements, particularly, aluminium content.

4. Conclusion

Two shape memory CuAlNi alloys with two different aluminium and constant nickel compositions are investigated by DSC and TGA methods. The characteristic temperatures of the thermoelastic martensitic transformation in primarily three thermal cycles are determined by analysing the DSC curves. It is found that increase of the aluminium content from 13.0 to 13.5 wt.% cause decrease in austenite peak (maximum) temperature from 155.1 ± 0.2 to $66.2 \pm 0.2\,^{\circ}C$ for the first thermal cycle but there are no considerable changes at these temperatures in the successive thermal cycles. Therefore, from the procedure of direct quench to the iced-brine water at $-3\,^{\circ}C$, sufficiently stabilized β-type martensite phases in polycrystalline alloys have been obtained. The investigations on the oxidation behaviours of these alloys have also been carried out by TGA method. From these investigations, the temperatures at which these alloys can be used without loss of their shape memory properties are estimated and the usable maximum temperature is obtained as $367.4 \pm 0.2\,^{\circ}C$ for the alloy with 3.0 wt.% Al content and $310.5 \pm 0.2\,^{\circ}C$ for the alloy with 13.5 wt.% Al content. It is also, found that the oxidation rate can be suppressed by increasing the aluminium content and the oxidation start temperature gets reduced.

References

[1] N. Kayalı, S. Çakmak, E. Artunç, O. Adıgüzel, J. de Phys. IV 5 (1995) 895–900.
[2] P.C. Clapp, How would we recognize a martensitic transformation if it bumped into us on a dark & austy night?, in: R. Gotthardt, J.V. Humbeeck (Eds.), Proceedings of the ICOMAT'95, Lausanne, Switzerland, 20–25 August, J. de Phys. IV 5 (1995) 11–19.
[3] R. Stalmans, J.V. Humbeeck, L. Delaey, Acta Metall. Mater. 40 (1992) 2921–2931.
[4] N. Kayalı, Martensite stabilization and ageing effects in CuZnAl alloys, PhD Thesis, Department of Physics, Firat University Graduate School of Natural and Applied Sciences, 1993, Turkey (in Turkish).
[5] C.M. Wayman, J. Metal, June (1980) 129–137.
[6] K. Halter, SMA household-applications from superelastic tooth brush to fully automated cat's toilet, in: R. Gotthardt, J.V. Humbeeck (Eds.), Proceedings of the of ICOMAT'95, Lausanne, Switzerland, 20–25 August, J. de Phys. IV 5 (1995) 1235–1248.
[7] R.V.N. Melnik, A.J. Roberts, K.A. Thomas, Comp. Mater. Sci. 18 (2000) 255–268.
[8] E. Cingolani, J. Van Humbeeck, M. Ahlers, Metall. Mater. Trans. A 30 (1999) 493–499.
[9] M.A. Morris, T. Lipe, Acta Metall. Mater. 42 (1994) 1583–1594.
[10] C. Picornell, R. Rapacioli, J. Pons, E. Cesari, Mater. Sci. Eng. A273-275 (1999) 605–609.
[11] Z.G. Wei, H.Y. Peng, D.Z. Yang, C.Y. Chung, J.K.L. Lai, Acta Mater. 44 (1996) 1189–1199.
[12] V. Recarte, R.B. Pérez-Saez, E.H. Bocanegra, M.L. No, J. San Juan, Mater. Sci. Eng. A273-275 (1999) 380–384.
[13] J. Garcia, J. Pons, E. Cesari, Sicripta Mater. 37 (1997) 1783–1788.
[14] H.E. Kissenger, J. Res. Natl. Bur. Stand. 57 (1956) 217–221.
[15] A.I. Kostov, Z.D. Zivkovic, Thermachim. Acta 291 (1997) 51–57.
[16] N. Kayalı, R. Zengin, O. Adiguzel, Metall. Mater. Trans. A 31 (2000) 349–354.
[17] C.M. Friend, Scripta Metall. 20 (1986) 995–1000.
[18] T. Lipe, M.A. Morris, Acta Metall. Mater. 43 (1995) 1293–1303.
[19] R. Zengin, The effect of stress and radiation on the shape memory behaviour in copper based alloys, PhD Thesis, Department of Physics, Firat University Graduate School of Natural and Applied Sciences, 2002, Turkey, (in Turkish).
[20] M.A. Morris, Acta Metall. Mater. 40 (1992) 1573–1586.
[21] J.R. Morris, R.A. Collins, G. Dearnaley, J. Phys. F Metal Phys. 8 (1978) 1333–1342.
[22] A. Stergiou, P. Tsakiropoulos, Intermetallics 5 (1997) 117–126.
[23] Y. Niu, Z.L. Zhao, F. Gesmundo, M. Al-Omary, Corrosion Sci. 43 (2001) 1541–1556.
[24] Y. Liu, F. Colin, P. Skeldon, G.E. Thompson, X. Zhou, H. Habazaki, K. Shimizu, Corrosion Sci. 45 (2003) 1539–1544.
[25] Z.E. Horvath, G. Peto, Z. Paszti, E. Zsoldos, E. Szilagyi, G. Battistig, T. Lohner, G.L. Molnar, J. Gyulai, Nuc. Inst. Meth. Phys. Res. B 148 (1999) 868–871.